Surgical Endoscopy (2019) 33:322–332
https://doi.org/10.1007/s00464-018-6362-2

DYNAMIC MANUSCRIPT

A reel mechanism-based robotic colonoscope with high safety and maneuverability

Dongkyu Lee[1] · Seonggun Joe[1] · Hyeongseok Kang[1] · Taeyoung An[1] · Byungkyu Kim[1]

Received: 2 April 2018 / Accepted: 10 July 2018 / Published online: 23 July 2018

Abstract

Background At present, the colonoscopy is the most common method of screening for colorectal cancer. However, endoscopists still encounter difficulties with intubation, primarily due to the structural diversity (e.g., path, shape, and size) and viscoelasticity of the colon. Therefore, well-trained, skillful operators are required to overcome these factors and operate colonoscopes without harming patients.

Objectives In our previous work, we presented a reel mechanism-based robotic colonoscope designed to mitigate the difficulties of conventional colonoscopies. Although we reported excellent mobile performance with respect to the robot, we did not provide an in-depth discussion concerning patient safety. Therefore, in this article, we propose a method of improving robot safety, and this is verified by investigating the static and dynamic forces acting on the colon. In addition, the maneuverability and safety of the robot in the in vitro condition are evaluated.

Methods The safety solution is provided by covering the robot's legs with silicone. To evaluate the results, the reaction force according to leg deformation is measured. Then, the force transmitted to the colon is also measured when the robot moves through various environments. Finally, a mobility test on an excised porcine colon is performed to simultaneously verify the robot's maneuverability and safety.

Results We verify that the static and dynamic force acting on the colon is less than the burst force of a human colon. In addition, the maneuverability of the robotic colonoscope shows reliable locomotion performance even with the soft material covering the legs; it has forward velocities of 9.552 ± 1.940 mm/s on a flat path.

Conclusion Owing to the reliable locomotion mechanism with the safety-securing silicone, the robot achieves high and reliable maneuverability without any scratches or perforations to the porcine colon.

Keywords Microrobot · Robotic colonoscope · Reel mechanism · High maneuverability · High safety · Locomotion test

Colorectal cancer (CRC) is the third most common cancer in the United States, and it can be reduced through early diagnosis [1–3]. As a diagnosis tool, colonoscopies have become the method of choice since the introduction of the colonoscope by Olympus in 1969 [4]. However, colonoscopies still have some drawbacks, particularly in the form of 'difficult colonoscopy' [5], which arises due to the difficulty of intubation and the necessity for skillful operators. With respect to the latter, successful intubation depends on the operator's ability to feel the colonoscope's correct movements and monitor progress via the real-time video coming from the image sensor in the distal tip. During the diagnosis, special handling techniques for unpredictable cases such as paradoxical motions, N loops and α loops are required [6, 7]. These problems stem from forcible intubation, complex configurations of the large intestine (e.g., the sigmoid colon), and the viscoelasticity of the lumen. Furthermore, an unskillful operator can create critical complications—e.g., bleeding and perforations. For example, with paradoxical motions, the operator continually intubates the colonoscope despite believing that the colonoscope is moving backward based on

Dongkyu Lee and Seonggun Joe have contributed equally to this work.

Electronic supplementary material The online version of this article (https://doi.org/10.1007/s00464-018-6362-2) contains supplementary material, which is available to authorized users.

✉ Byungkyu Kim
bkim@kau.ac.kr

[1] School of Aerospace and Mechanical Engineering, Korea Aerospace University, Goyang-si, Republic of Korea

the real-time video. In this case, if the operator cannot detect the situation and forcibly intubates, the corner becomes a loop and the patient will feel pain due to the extension of the large intestine. Such drawbacks result in not only discomfort and medical complications, but also excessive physical exertion on the part of the operator ('endoscopist sweat') [5]. In addition, some endoscopists show poor cecum intubation rates, especially in European countries [8].

Most researchers have associated the drawbacks with forcible intubation. Therefore, several solutions such as robotic colonoscopes and capsule endoscopes (CEs) have been proposed [9, 10]. Robotic colonoscopes generally use two approaches—biomimetic (e.g., earthworm [11–14] and inchworm [15–18] approaches) and mechanical (e.g., link mechanisms [19], screw mechanisms [20], pneumatic devices [21], and caterpillar-based mechanisms [22, 23]). However, all of these attempts have suffered from safety limitations, and their locomotion performance has been lower than that of conventional colonoscopies. Even though a few approaches have achieved promising results and have been commercialized [24], they have not been able to substitute conventional colonoscopes completely due to lack of treatment tools. In addition, some of the new robotic colonoscopes now serve as assisting devices for endoscopist-guided intubation [25].

In our previous study, we presented a robotic colonoscope based on a simple and reliable reel-based mechanism, and it was actuated by an external motor [26]. The robot not only exhibited high maneuverability employing an external power source, it also demonstrated the potential to carry out treatment functions by securing structural spare space in the robot body. However, because the robot used a rigid material for the contact components (legs), there was concern that the components would damage the internal wall despite the absence of red marks and perforations after the in vitro test. In this paper, therefore, the safety of the robot is improved by harnessing a soft material for the legs. The mobile performance is then verified in the in vitro test. To evaluate the safety of the contact components, two analyses are carried out—an investigation of the reaction force according to the deformation of the legs (static experiment), and an investigation of the transmitted force from the robot to the colon while the robot operates in an excised porcine colon (dynamic experiment). Finally, an in vitro test using an excised porcine colon is conducted to evaluate the locomotion performance for a large intestine. In the in vitro test, the motion of the robot in the excised porcine colon is directly observed using a USB endoscope camera module.

Materials and methods

Robot design

The robotic colonoscope system consists of a robotic colonoscope (i.e., robot), a reel controller and a Bowden cable [27], as shown in Fig. 1. The robot is designed to move in a human body along the large intestine, and it includes the following components: an outer cylinder, inner cylinder, friction ring, six legs covered by a soft material, counter spring, guide bars, body, and end cap. The two cylinders move sequentially because they structurally constrain each other. The six legs are installed at the outer cylinder, and they are deployed and folded via the inner cylinder due to their structural constraints. The legs are fabricated with stainless steel and covered with silicone to secure the safety of the patient. The friction ring interrupts the motion of the two cylinders and causes the legs to deploy completely. The counter spring causes the cylinders to push to the original position when the reel releases the tension wire. The guide bars are positioned between the two cylinders and result in an exact longitudinal motion. The reel controller is positioned outside the human body so that a high-power BLDC motor can be employed. The reel controller consists of the BLDC motor with a gearhead and encoder as well as a reel attached with the tension wire. The Bowden cable contains the tension wire that pulls the inner cylinder, helical steel wire that supports the endcap and reel bracket, and a silicone sheath to prevent damage to the large intestine.

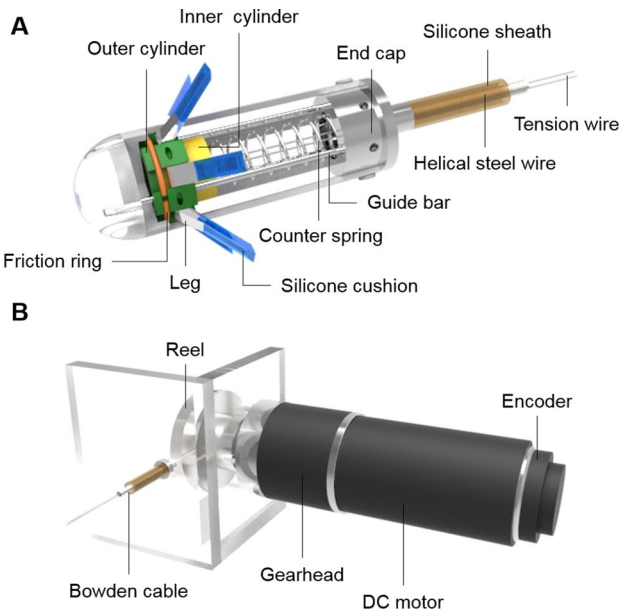

Fig. 1 Schematic of the proposed robotic colonoscope. **A** Robotic colonoscope. **B** Reel controller

The human colon consists of five segments—the ascending colon, transverse colon, descending colon, sigmoid colon, and rectum—and their average diameters are 49.1, 42.2, 33.2, 33.2, and 37.5 mm, respectively [28]. The outer diameter of the robot when the legs are fully deployed is 33 mm, which is less than the reported minimum diameter of the human colon. In addition, the robot diameter excluding the soft material on the legs is designed to be 30.5 mm. Therefore, geometrically, the robot cannot cause damage to the colon. As a result, we can expect that damage to the patient will not occur with the robot design parameters when considering the colon's open lumen sizes in Fig. 2.

Locomotion mechanism

The reel rotation drives the robot as shown in Fig. 3. The detailed locomotion principle is as follows:

A. The robot is in its initial state in the human colon.
B. When the reel rotates clockwise (CW) to wind the tension wire, the inner cylinder moves backward, and the legs are deployed due to their structural constraints.

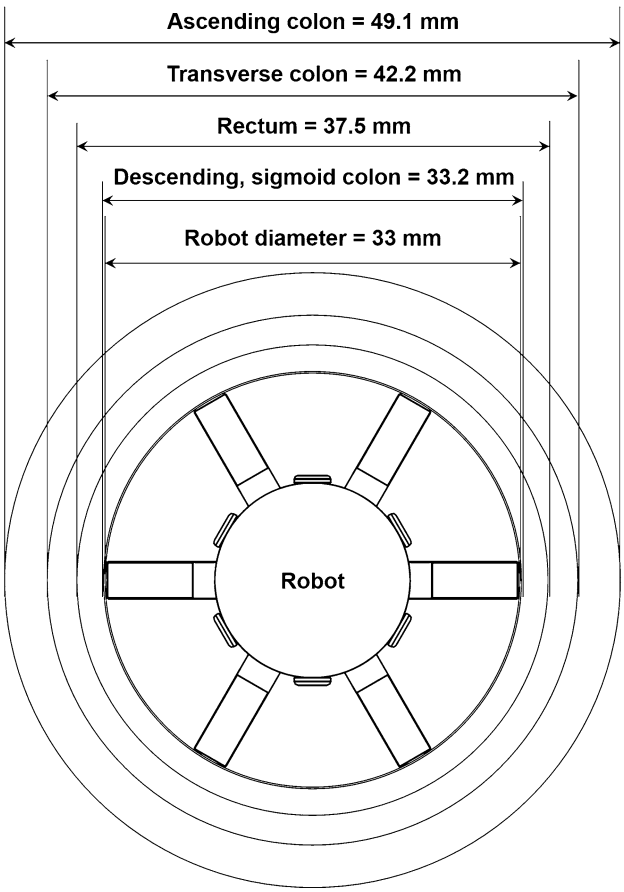

Fig. 2 Diameter of the robot (front view) as compared to the human colon

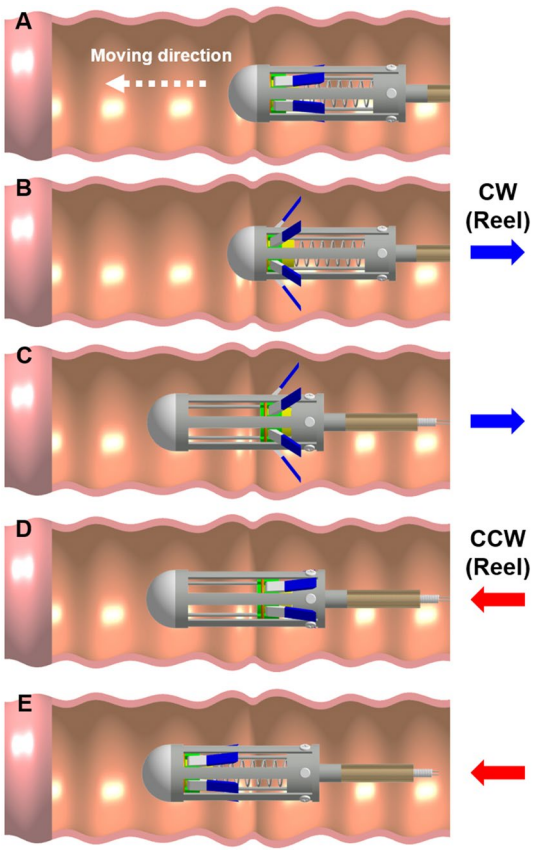

Fig. 3 Locomotion principle of the robotic colonoscope; the arrow denotes the moving direction of the tension wire

C. While the tension wire continually pulls the inner cylinder via the reel rotation, the robot body advances forward due to the reaction force of a helical steel wire such as a general Bowden cable.
D. When the maximum stroke of the robot is reached, the reel rotates counter clockwise (CCW), and the tension wire unwinds. After the inner cylinder moves forward via the counter spring, the legs fold as per the inverse of the aforementioned structural constraints.
E. The cylinders return to the original position via the counter spring. The steps repeat, and the robot moves forward.

The robot velocity is controlled by the motor speed, which is set at 150 rpm after considering the stability of the robot as reported in the previous article [26]. The free length of the counter spring is fixed at 40 mm considering the buckling effect [29], and the spring is fabricated with a Hard Drawn ASTM A227 wire [30].

To analyze the robot's velocity, the velocity of the mobile element, which comprises the outer cylinder, the inner cylinder, and the six legs, should be calculated. The

equation to express the velocity of the mobile element (V_{mobile}) is as follows:

$$V_{\text{mobile}} = \frac{V_{\text{motor}}}{2} \times \frac{l_{\text{output}}}{l_{\text{input}}} = \frac{V_{\text{motor}}}{2} \times \frac{l_{\text{input}} - \left(l_{\text{dead}} + l_{\text{lumen}} + \alpha\right)}{l_{\text{input}}}, \quad (1)$$

where V_{motor} is the motor speed, l_{output} is the real output stroke used to advance the robot, l_{input} is the ideal input stroke from the stepper motor, l_{dead} is a structurally generated dead stroke under the leg deployment procedure, l_{lumen} is the loss from the loads on the mechanical components under the operating conditions in a particular lumen, and α is a variable that changes depending on the viscoelasticity and drag coefficient of the colon. Considering ideal conditions, l_{lumen} and α are ignored because they are affected by the environmental conditions.

Because the designed control system has a time delay (t_{delay}) of 250 ms considering the signal processing duration and the moment of inertia caused by a sudden change in the motor rotation direction, the working time should be revised to obtain the exact robot velocity. Therefore, we can obtain the robot velocity based on Eq. (1) as follows:

$$t_{mobile} = \frac{l_{output}}{V_{mobile}} \quad (2)$$

$$V_{robot} = \frac{l_{output}}{t_{mobile} + t_{delay}}. \quad (3)$$

Using Eq. (3), the ideal robot velocity is calculated as 30.464 mm/s with the motor speed of 150 rpm. This is appealing performance compared to a conventional robotic colonoscope [8–22].

Control system

The control system of the robotic colonoscope is composed of a reel controller, an encoder (No. 225785, Maxon motor), a motor positioning controller (EPOS 70/10, Maxon motor), and a PC-based control panel. When the demand position is sent to the control panel as a rotation angle, the motor starts rotating CW to move the mobile element backward. Then it is controlled by a PID controller, which is set up using EPOS User Interface software (EPOS Studio 3.1 revision 2, Maxon motor). Each gain value is determined based on the Ziegler–Nichols method [31] and modified through an experiment. As a result, the P, I, and D gains are set to 1181, 9115, and 1862, respectively, for the position tuning. The other gains used for the current and velocity tuning are presented in Table 1. The actual position properly follows the set position, as shown in Fig. 4. When the CW motor rotation finishes, a time delay of 250 ms is allocated to secure the calculation and signal processing time, as well as to minimize the moment of inertia caused by the sudden change in the motor rotation direction. The motor subsequently rotates CCW with the aforementioned gain values to return the mobile element to its original position. Consequently, the robot locomotion is controlled by repeatedly implementing the control sequence (CW rotation-delay-CCW rotation).

Table 1 PID gain values for current, velocity, and position control

	Current	Velocity	Position
P	390	4513	1181
I	73	1293	9115
D	–	–	1862

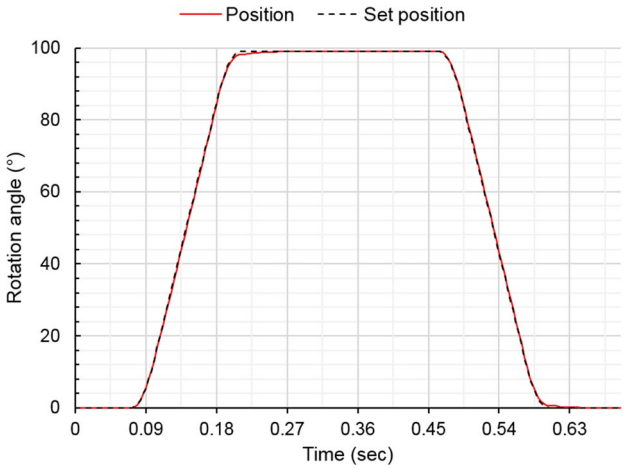

Fig. 4 Motor position following of PID controller

Robotic colonoscope system

The robotic colonoscope system contains the robotic colonoscope, reel controller, Bowden cable between the robotic colonoscope and controller, and the control system, as shown in Fig. 5. The robot is fabricated with aluminum 6061 and has a diameter of 16 mm and length of 49 mm, which includes a front dome. The six legs are fabricated with stainless steel to secure structural stability, and they are covered with silicone to improve operating safety. The reel controller consists of a reel with a diameter of 25 mm, a BLDC motor with a gear box (6:1) and an encoder (No. 148867, No. 260551, No. 225,785, Maxon Motor). The motor positioning controller (EPOS 70/10, Maxon Motor) is employed to control the motor and read signals from the encoder. The Bowden cable with a length of 1 m contains a spring steel helical wire, stainless steel tension wire 0.6 mm in diameter, and a silicone sheath 5 mm in diameter. The control system is designed to compensate for the loss of torque and position

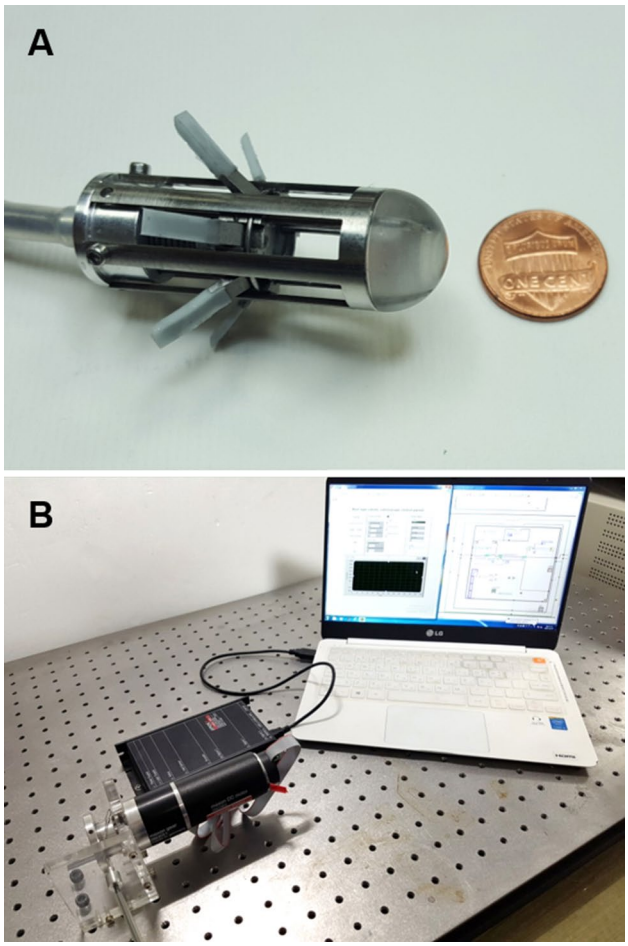

Fig. 5 Fabricated robotic colonoscope system. **A** Robotic colonoscope. **B** Reel controller and control system with robot control panel on personal computer

at the motor due to environmental factors such as those mentioned in the previous section.

Leg design with soft material

The driving component is critical with respect to patient safety because it can cause damage to the colon. Therefore, each of the robot's legs consists of one rigid and one soft part. The rigid part is fabricated with stainless steel. Its end serves as the backbone for the soft part. As shown in Fig. 6, Cases A and B have different shaped backbones, which help determine durability and safety. Case A is designed to absorb more contact force by increasing the thickness of the soft part. Case B is more durable because the soft part completely envelops the backbone. Commercial silicone with high hardness (KE-1600 by Shin-Etsu Chemical Co., Ltd.) is used for the soft part. The silicone hardness is rated as durometer A 45 after the standard cure time elapses, and it can increase up to 70 via an aging process (30 min at

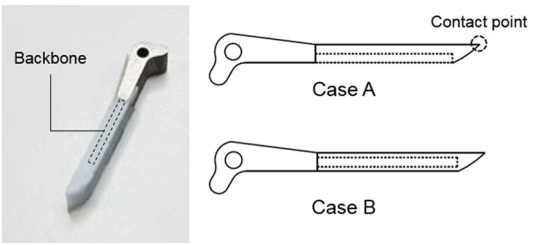

Fig. 6 Fabricated leg covered with silicone (Light blue color). (Color figure online)

150 °C). Therefore, every leg used in the experiment undergoes the aging process to increase the silicone hardness. In the experiment, Case C, which does not use silicone, is fabricated to facilitate a comparison for Cases A and B.

Experimental setup to investigate the physical properties of the leg

The experimental setup employed to measure reaction force of the leg according to deformation is shown in Fig. 7. The reaction force measured between the Bowden cable and the reel bracket is the force that is transmitted toward robot. To replicate the exact displacement of leg deformation, a one-axis micro-stage is employed. A load cell (Model CB1-K3 (Cap. 3 kgf), DACELL Co.) is used to measure the reaction force from the leg. The leg is installed at a degree of 52°, which mimics the deployed state for locomotion. The leg installation component is fabricated using a 3D printer (Objet24, Stratasys, Eden Prairie, MN, USA) and the material is a rigid white material (VeroWhitePlus, Stratasys, Eden Prairie, MN, USA). When the reaction force is measured, the leg installation component for each leg (Cases A, B, and C) is installed under the load cell, as shown in Fig. 7B. The force can be confirmed using an indicator (DN-50W, DACELL Co.).

Experimental setup to investigate dynamic force between leg and the excised porcine colon

In addition, we investigate the dynamic force from the robot to the colon when the robot operates. As shown in Fig. 8, the robot is positioned in an excised porcine colon and a signal is given to the motor. The robot is operated using the proposed control system, and a load cell (Model CB1-K3 (Cap. 3 kgf), DACELL Co.) is installed between the Bowden cable and reel bracket. The load cell measures the total amount of transmitted force from the control system to the robot when the robot is operated. A DAQ board (NI USB-6281) is utilized to obtain signals from the load cell, and LabVIEW software converts the signals into force values so that force variations can be observed by user in real time.

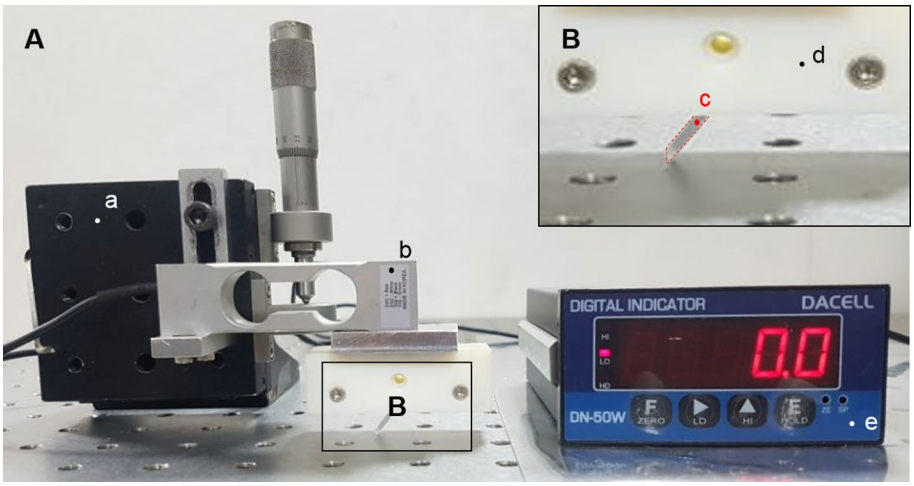

Fig. 7 Experimental setup for the reaction force measurement of the leg; **A** Micro-stage, **B** Loadcell, **C** Leg, **D** Leg installation component, **E** Indicator

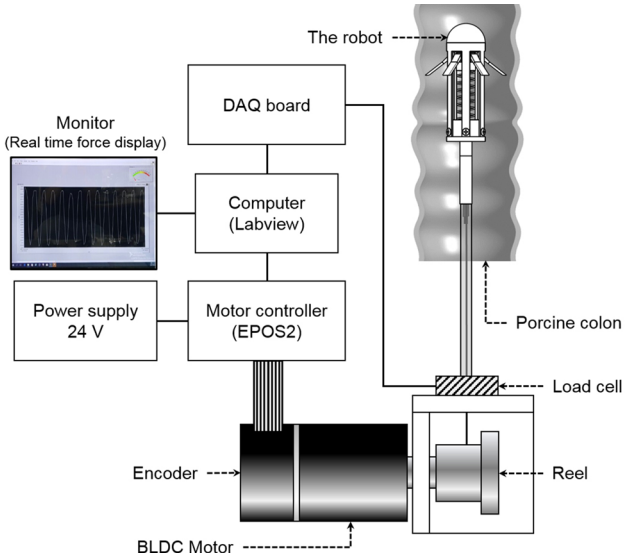

Fig. 8 Experimental setup to measure the reaction force when the robot moves in a porcine colon

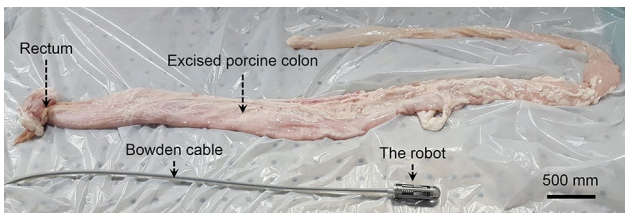

Fig. 9 Robot and excised porcine colon for the in vitro test

Experimental setup for in vitro test

In the in vitro test (Fig. 9), an excised porcine colon is utilized to imitate a real human colon. The porcine colon is prepared within 12 h from extraction and has a rectum. The configuration of the colon in the locomotion test is determined considering a human large intestine. The input motor speed is set to 150 rpm for all locomotion test cases, and lubricant oil (TF2 lubricant with Teflon®, Weldtite 03034, WELDTITE, UK) is filled in the Bowden cable to minimize friction between the helical wire and the silicone sheath, as well as between the helical wire and the tension wire.

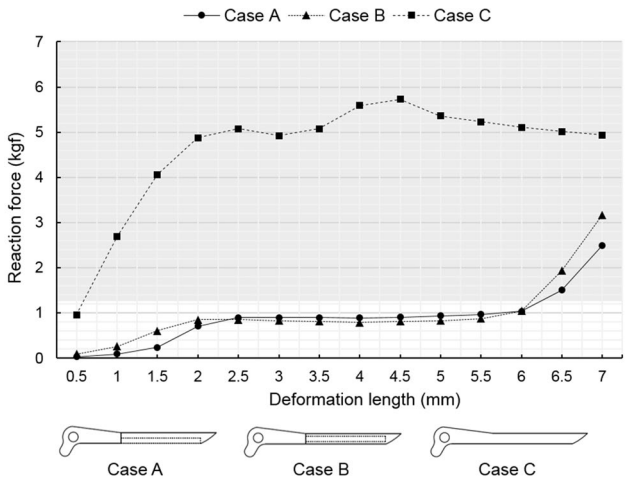

Fig. 10 Experimental results for the reaction force measurement of the leg; the gray zone expresses dangerous levels with respect to the mechanical properties of the human colon (> 1.22 kgf)

Results

Static and dynamic force on the colon

Contact force between the legs and the colon wall is measured using the experimental setup in Fig. 7. In the experiment, three leg types in Fig. 10 are utilized—Cases A and B and Case C without the soft material. Obviously, although Case C

would cause damage to the colon wall with repeated contact, the measurement data for C are only used as a control group. The measurements are conducted up to a deformation length of 7 mm along the vertical direction, which causes the plastic deformation of the leg.

The experimental results are shown in Fig. 10. The silicone-covered legs (Cases A and B) show much lower levels of force than Case C, and the maximum difference between them is 4.91 kgf. In particular, considering the reported burst force of the human colon (shown in Table 2), Cases A and B show good results when the deformation length is < 6 mm. In addition, the reaction force with a deformation of 1.5 mm—the thickness of the silicone cover in the vertical direction at the installation condition—is measured as 0.611 kgf, which is less than half of the minimum burst force of the human colon. In Case C, the contact force exceeds the burst force of the human colon when the deformation length is over 1 mm. Conclusively, the silicone-covered leg significantly increases the safety of the driving component, and we can anticipate that the safety of the robot would increase by employing either Case A or B. For Case A, the repeated action of the leg might cause the silicone to disassemble from the leg due to the small contact surface. Therefore, case B is installed for the in vitro test.

Although the safety of the robot components is verified statically, the dynamic force acting on the colon could cause scratches or perforations while the robot locomotes. Therefore, the force being transmitted to the robot using the Case B components is investigated to confirm the dynamic influence on the colon with the experimental setup in Fig. 8. The experiment is implemented for three environments—(1) ideal, which is measured without any obstacles, and a minimum amount of force is required to operate the robot; (2) open lumen, which is measured in the colon hanging in the air; and (3) closed lumen, which is measured in the colon laid out on the test table. The sampling frequency is set to 1 kHz, and the resampling frequency is set to 0.1 kHz.

As shown in Fig. 11, the difference between the maximum value of the ideal condition (2.180 kgf) and open lumen (2.871 kgf) is measured as 0.691 kgf, which stems from the special characteristics of the colon, including deformability and slipperiness. The maximum transmitted force to the robot in the closed lumen is measured as 3.601 kgf, which is 1.65-fold higher than the force in the ideal condition. Because the closed lumen interrupts the robot's advance, the transmitted force in the closed lumen is higher than in the open lumen. Conclusively, in the closed lumen, the contact force toward

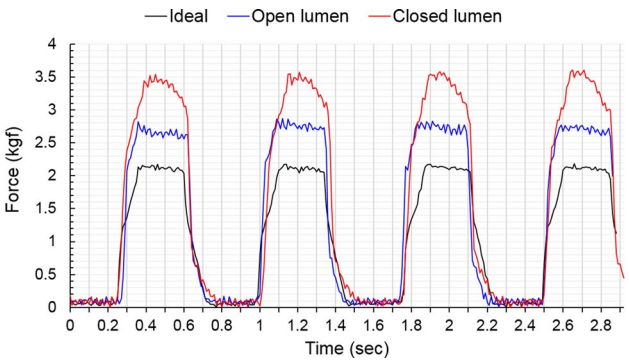

Fig. 11 Experimental result of dynamic influence from the robot to the colon

the colon from the six legs is calculated as 1.421 kgf, which is the difference between the transmitted force (3.601 kgf) in the closed lumen and the maximum value of the ideal condition (2.180 kgf). Therefore, the contact force of each leg while in the colon is 0.237 kgf, which is < 20% of the burst force of the human colon.

Locomotion test in porcine colon

A locomotion test of the robotic colonoscope system with the safety-securing component is implemented in the porcine colon with three configurations, as shown in Fig. 12. The paths are determined considering a real large intestine configuration, which includes the closed lumen before air insufflation (Fig. 12A) and inclining lumen (Fig. 12B, C) [28]. All of the results for the locomotion test are analyzed using open source video analysis software (Tracker version 4.11.0, Douglas Brown, Open Source Physics) [33].

As shown in Fig. 13, the robotic colonoscope achieves the fastest result for the flat path at 9.552 ± 1.940 mm/s. With the inclining path, the velocities are 7.140 ± 1.355 and 5.091 ± 0.643 mm/s at 30° and 60°, respectively. For all cases, neither perforations nor damage is observed after the in vitro test.

Discussion

As mentioned in the above section, we expect that the proposed robot components can improve operating safety and prevent damage toward the colon wall. To confirm the

Table 2 Burst force of wall of the large intestine taken from European and African subjects for each segment [32]

	Ascending colon	Transverse colon	Descending colon	Sigmoid colon
Burst force (kgf)				
European	1.38 ± 0.82	1.22 ± 0.70	1.24 ± 0.66	1.27 ± 0.65
African	1.80 ± 0.65	1.69 ± 0.59	1.64 ± 0.50	1.62 ± 0.66

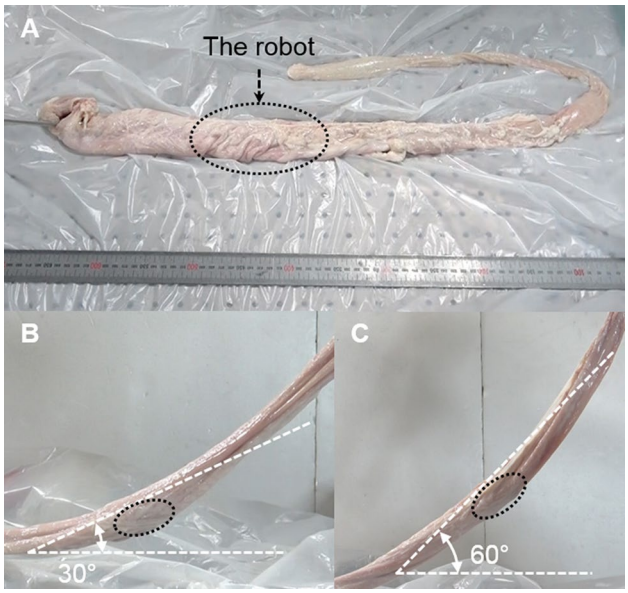

Fig. 12 In vitro test in porcine colon. **A** Flat path, **B** Inclining path (30°), **C** Inclining path (60°)

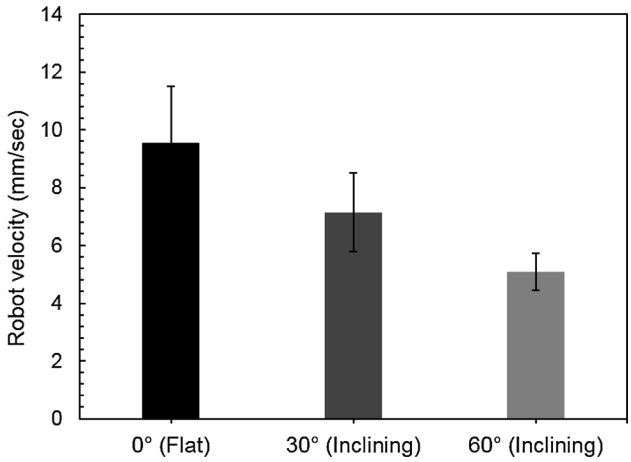

Fig. 13 Robot velocities for all experimental cases in the article (motor speed = 150 rpm)

influence of the safety-securing component, the robot locomotion is recorded using a USB endoscope camera module (2.0 Megapixel CMOS, diameter = 8 mm), as shown in Fig. 14. Also, the USB endoscope camera module is placed at the front and rear of the robot situationally.

As shown in Fig. 15A, B, the robot advance is observed in the porcine colon. Bending of the silicone is observed, and we can expect that this bending will prevent damage to the colon (Fig. 15C, white dashed circle). In addition, we cannot find perforations or red marks in the locations contacted by the leg (Fig. 15D, yellow dashed circle). Conclusively, the robotic colonoscope guarantees safety based on the video clip (Fig. 15) as well as the previous analysis with the static and dynamic experiments.

In terms of the maneuverability of the robot, the experimental results show lower values than the designed robot velocity of 30.464 mm/s. The decrease stems from the colon characteristics and the safety component. The gastrointestinal wall is weak and deformable, and it is slippery in a different manner than general pipes. In detail, the submucosa layer is more easily elongated than other layers such as the mucosa, muscular, and serosa [34]. Although the driving component of the robotic colonoscope realizes clear contact with the mucosa, elongation of the submucosa causes the robot to slip, and stroke loss is incurred. In addition, the mucous secretion makes the internal wall slippery. Therefore, the decrease in speed might be directly connected to the lack of clear contact between the colon wall and the driving components [35]. Clearly, the robotic colonoscope experiences difficulty in advancing in the real colon. Moreover, in the case of the inclining path, the robot cannot avoid slipping in the colon because of the gravitational forces.

Second, the deformation of the silicone leg-end tip results in stroke loss, which leads to a decrease in robot velocity. For example, for the 30° inclining path, the robot velocity is reduced by more than half compared to the velocity of 18.77 ± 3.42 mm/s in the previous study [23]. In that case, the sharp leg-end tip achieved clear strokes based on the exact support between the colon walls. However, in this study, the leg covered with silicone in the proposed robot is deformed, and this causes slips in the lumen, which is linked directly to the stroke loss. Nevertheless, the simplified structure and effective mechanism-based robotic colonoscope system achieves better mobile performance (9.552 ± 1.940 mm/s) than reported robotic colonoscopes, as shown in Table 3. Even the worst case (5.091 ± 0.643 mm/s for the 60° inclining path) is faster than any other reported results. Conclusively, the robot achieves higher levels of safety based on the successful safety analysis and locomotion tests using the porcine colon, and it simultaneously retains high maneuverability.

Conclusion

This paper presents a reel mechanism-based robotic colonoscope which realizes high maneuverability as well as improves patient safety. The proposed mechanism is more effective than reported robotic colonoscopes due to its simplified structure and power transmission method, which uses a Bowden cable with a high-capacity motor that is external to the body. In order to provide safety while keeping high maneuverability, the robot's legs are covered with silicone. As a result, the static and dynamic forces acting on the colon by the legs are 0.611 kgf with a deformation of 1.5 mm and

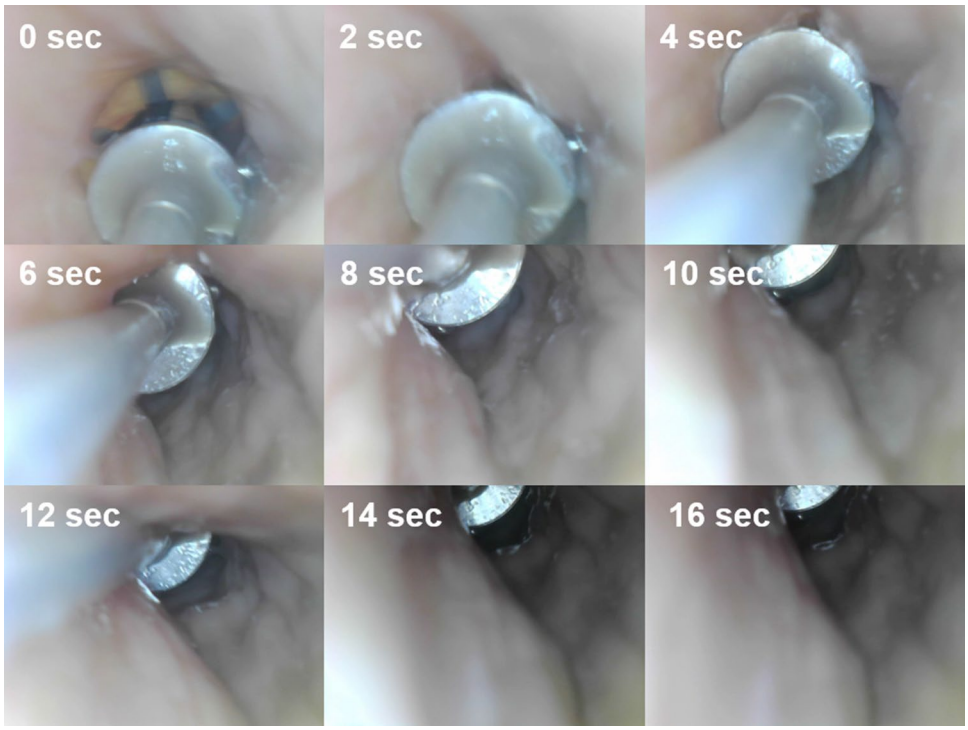

Fig. 14 Video screen shots of the robot's locomotion in the excised porcine colon with an interval of 2 s; the camera is positioned at the rear of the robot and a motor speed of 150 rpm is employed for this video clip

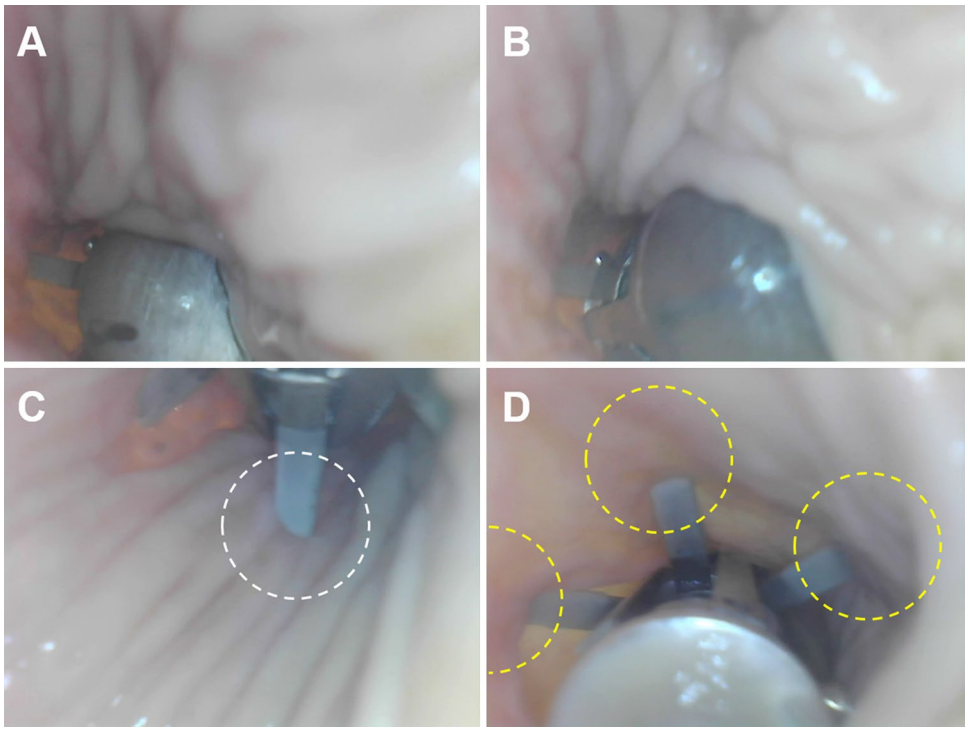

Fig. 15 Video screen shots of the robot's locomotion in the excised porcine colon. **A**–**C** Front view of the robot. **D** Rear view of the robot

0.237 kgf, respectively, which are much less than the burst force of a human colon. In addition, maneuverability is evaluated under various environments mimicking the configurations of the human colon to investigate locomotion loss since the silicone covering the legs has a soft, slippery surface compared to steel. The robot equipped with the silicone-covered legs moves at 9.552 ± 1.940 mm/s on the flat path, 7.140 ± 1.355 at 30° and 5.091 ± 0.643 mm/s at 60°. Consequently, the proposed robotic colonoscope is still faster than any other reported robotic colonoscopes. Conclusively, we

Table 3 Reported maximum velocities of robotic colonoscopes

Ref. No.	Bernth JE et al. [11]	Alcaide JO et al. [12]	Heung HL [13]	Wang K et al. [14]
Max velocity (mm/s)	1.21	4	1.5	2.20
Ref. No.	Kim B et al. [15]	Wang K et al. [17]	Lee J et al. [20]	Sliker LJ et al. [22]
Max velocity (mm/s)	3.16	3.25	2.24	3

are able to enhance safety while keeping high maneuverability by employing a reel mechanism and silicone-covered legs.

Compliance with ethical standards

Disclosures Dongkyu Lee, Seonggun Joe, Hyoeng-Seok Kang, Taeyoung An, and Byungkyu Kim declare no conflicts of interest.

References

1. U.S. Cancer Statistics Working Group (2010) United States Cancer Statistics: 1999–2007 incidence and mortality web-based report. Department of Health and Human Services, Centers for Disease Control and Prevention, and National Cancer Institute, Atlanta
2. Nakao SK, Fassler S, Sucandy I, Kim S, Zebley DM (2013) Colorectal cancer following negative colonoscopy: is 5-year screening the correct interval to recommend? Surg Endosc 27(3):768–773
3. Moore JS, Aulet TH (2017) Colorectal cancer screening. Surg Clin 97(3):487–502
4. Dafnis G (2006) A novel technique for endoscopic snare polypectomy using a duodenoscope in combination with a colonoscope for the inaccessible colonic polyp. Endoscopy 38(03):279–281
5. Witte TN, Enns R (2007) The difficult colonoscopy. Can J Gastroenterol 21(8):487–490
6. Waye JD, Rex DK, Williams CB (eds) (2008) Colonoscopy: principles and practice. Wiley, Hoboken
7. Yoshida N et al (2009) Endoscopic submucosal dissection for colorectal tumors: technical difficulties and rate of perforation. Endoscopy 41(09):758–761
8. Bowles CJA, Leicester R, Romaya C, Swarbrick E, Williams CB, Epstein O (2004) A prospective study of colonoscopy practice in the UK today: are we adequately prepared for national colorectal cancer screening tomorrow? Gut 53(2):277–283
9. Dario P, Mosse CA (2003) Review of locomotion techniques for robotic colonoscopy. In: Proceedings of the ICRA'03. IEEE International Conference on Robotics and Automation, 2003. 1:1086–1091
10. Ciuti G et al (2016) Frontiers of robotic endoscopic capsules: a review. J Microbio Robot 11(1–4):1–18
11. Bernth JE, Arezzo A, Liu H (2017) A novel robotic meshworm with segment-bending anchoring for colonoscopy. IEEE Robot Autom Lett 2(3):1718–1724
12. Alcaide JO, Pearson L, Rentschler ME (2017) Design, modeling and control of a SMA-actuated biomimetic robot with novel functional skin. In: IEEE International Conference on Robotics and Automation (ICRA), 2017, pp 4338–4345
13. Heung H, Chiu PW, Li Z (2016) Design and prototyping of a soft earthworm-like robot targeted for GI tract inspection. In: IEEE International Conference on Robotics and Biomimetics (ROBIO), 2016, pp 497–502
14. Wang K, Ma J, Wang F, Wang Z, Yan G, Zhou Y (2017) Full-driving soft robotic colonoscope in compliant colon tissue. J Med Eng Technol 41(8):662–669
15. Kim B, Lim HY, Park JH, Park JO (2006) Inchworm-like colonoscopic robot with hollow body and steering device. JSME Int J C-Mech Sy 49(1):205–212
16. Poon CC, Leung B, Chan CK, Lau JY, Chiu PW (2016) Design of wormlike automated robotic endoscope: dynamic interaction between endoscopic balloon and surrounding tissues. Surg Endosc 30(2):772–778
17. Wang K, Ge Y, Jin X (2013) A micro soft robot using inner air transferring for colonoscopy. In: IEEE International Conference on Robotics and Biomimetics (ROBIO), 2013, pp 1556–1561
18. Lim J, Park H, An J, Hong YS, Kim B, Yi BJ (2008) One pneumatic line based inchworm-like micro robot for half-inch pipe inspection. Mechatronics 18(7):315–322
19. Kim B et al (2003) Functional colonoscope robot system. In: Proceedings of the ICRA'03. IEEE International Conference on Robotics and Automation, 2003, pp 1092–1097
20. Trovato G et al (2010) Development of a colon endoscope robot that adjusts its locomotion through the use of reinforcement learning. Int J Comput Assist Radiol Surg 5(4):317–325
21. Dehghani H, Welch CR, Pourghodrat A, Nelson CA, Oleynikov D, Dasgupta P, Terry BS (2017) Design and preliminary evaluation of a self-steering, pneumatically driven colonoscopy robot. J Med Eng Technol 41(3):223–236
22. Sliker LJ, Kern MD, Schoen JA, Rentschler ME (2012) Surgical evaluation of a novel tethered robotic capsule endoscope using micro-patterned treads. Surg Endosc 26(10):2862–2869
23. Lee D, Joe S, Choi J, Lee BI, Kim B (2016) An elastic caterpillar-based self-propelled robotic colonoscope with high safety and mobility. Mechatronics 39:54–62
24. Patel N, Darzi A, Teare J (2015) The endoscopy evolution: 'the superscope era'. Frontline Gastroenterol 6(2):101–107
25. Shike M et al (2008) Sightline ColonoSight system for a disposable, power-assisted, non-fiber-optic colonoscopy (with video). Gastrointest Endosc 68(4):701–710
26. Lee D, Joe S, Jung JH, Kim JU, Kim B (2017) A simple and reliable reel mechanism-based robotic colonoscope for high mobility. Proc Inst Mech Eng Part C. https://doi.org/10.1177/0954406217723941
27. Jeong U, In H, Lee H, Kang BB, Cho KJ (2015) Investigation on the control strategy of soft wearable robotic hand with slack enabling tendon actuator. In: IEEE International Conference on Robotics and Automation (ICRA), 2015, pp 5004–5009
28. Sadahiro S, Ohmura T, Yamada Y, Saito T, Taki Y (1992) Analysis of length and surface area of each segment of the large intestine according to age, sex and physique. Surg Radiol Anat 14(3):251–257
29. Nisbett J, Budynas R (2008) Shingley's mechanical engineering design. Mc- Graw-Hill, New York

30. Grijalba YL, Ramirez AJ (2015) Comparison of double torsion springs with anticorrosive coating obtained from manual production against those obtained from an automated forming prototype. In: 15th congreso nacional de ingenieria electromecanica y de sistemas (CNIES 2015) pp 19–23
31. Meshram PM, Kanojiya RG (2012) Tuning of PID controller using Ziegler-Nichols method for speed control of DC motor. In: International Conference on Advances in Engineering, Science and Management (ICAESM), 2012, pp 117–122
32. Watters DA, Smith AN, Eastwood MA, Anderson KC, Elton RA, Mugerwa JW (1985) Mechanical properties of the colon: comparison of the features of the African and European colon in vitro. Gut 26:384–392
33. Amador GJ, Matherne M, Mathews M, Gorb SN, Hu DL (2017) Honey bee hairs and pollenkitt are essential for pollen capture and removal. Bioinspir Biomim 12(2):026015
34. Egorov VI, Schastlivtsev IV, Prut EV, Baranov AO, Turusov RA (2002) Mechanical properties of the human gastrointestinal tract. J Biomech 35(10):1417–1425
35. Accoto D et al (2001) Measurements of the frictional properties of the gastrointestinal tract. In: World Tribology Congress Vol 3, p 7